A New Shipborne Microwave Refractometer for Estimating the Evaporation Flux at the Sea Surface

J.-Y. DELAHAYE,* C. GUERIN,* J. P. VINSON,* H. DUPUIS,[+] A. WEILL,* H. BRANGER,[#]

L. EYMARD,* J. LAVERGNAT,* AND G. LACHAUD[@]

CETP (CNRS), Velizy, France
[+] *DGO (CNRS), Bordeaux, France*
[#] *IRPHE (CNRS), Parc Scientifique et Technologique de Luminy, Marseille, France*
[@] *CNRM/Meteo France, Toulouse, France*

ABSTRACT

After a brief description of humidity measurement and a short presentation of methods of microwave refractometry for evaporation flux, a new X-band refractometer system is presented. Based on a new design and a new material for the microwave cavity, it does not need calibration for refractive index variations because of its reduced thermal time constant.

The new device has been combined with a sonic anemometer and traditional mean meteorological measurements on a 12-m shipborne mast. It has been found to be very efficient for obtaining humidity fluctuations and fluxes in the CATCH 97 (Couplage avec l'ATmosphère en Conditions Hivernales) and FETCH 98 (Flux, Etat de la mer et Télédétection en condition de fetCH variable) experiments under various wind and stability conditions. The inertial subrange is of very high quality. To first order, the evaporation flux and refractive index flux are very similar. In extreme meteorological conditions, such as those encountered during CATCH, the sensible heat flux contribution must be determined independently.

A great advantage of the system is that the contamination by salt, as is typical for other devices at sea, has been found to be negligible for the conditions encountered.

1. Introduction

Measurement of humidity fluctuations over the sea from a fixed (e.g., tower) or a mobile (e.g., ship) platform is very difficult due to the problem of contamination of the various instruments used (salt, particles, aerosol contamination) and the problems of reliability. The accurate and reliable measurement of humidity fluxes and humidity fluctuations is nonetheless a very important goal when studying ocean–atmosphere exchanges, and measurements of the mean specific air humidity ratio of water vapor mass have been attempted for many years.

Different techniques and devices for estimating humidity have been developed since the beginning of the 20th century, including:

- humidity absorption by hygroscopic substances to estimate absolute humidity,
- wet bulb thermometry (measurement of the temperature difference between a humidified thermometer and a "dry reference thermometer") or dewpoint measurements (dew temperature measurement when a dew deposit appears on a cooled surface) to estimate relative humidity.

Many systems were built, and progress in electronics has brought about new devices often using other kinds of properties such as frequency variation of piezoelectric systems, the variation of the electric capacitance as a function of humidity, and systems measuring the absorption of emitted infrared and UV radiation.

A slow measurement of humidity can now be carried out in the lower atmosphere (above the ocean) for humidity variations between 20% and 100%, with a relative accuracy between 5% and 10%. For a comprehensive analysis of the state of art at the end of the 1970s, see McKay (1978) or Coantic and Friehe (1980). Saturation phenomena (hysteresis) due to precipitation or response changes related to pollution by particles are now relatively well understood. This is not the case for fast-response humidity measurements at the sea surface, which remain a challenge today. Humidity is often large at the sea surface, where an important amount of particulate, especially salt, contamination is present.

Corresponding author address: Dr. Jean-Yves Delahaye, Centre d'études des Environnements Terrestre et Planétaires, 10/12 avenue de l'Europe, 78140 Vélizy, France.
E-mail: delahaye@cetp.ipsl.fr

For mean humidity measurement, a coarse time response of 10 s or more is acceptable, but for measuring fluxes, one needs a finer time response. When using, for example, the inertial dissipation method, a time response of less than 100 ms is required, which corresponds to a distance scale of about 2.5 m at a wind velocity of 25 m s^{-1}. A good sensitivity in the humidity fluctuation is also required, and a noise level typically smaller than 20 mg m^{-3} is a reasonable goal (Auble and Meyers 1992).

The two following techniques are mainly used to estimate humidity fluctuations (see, e.g., the paper by Priestley and Hill (1985):

- Lyman-alpha systems that involve ultraviolet radiation absorption in the water vapor absorption band (Tillman 1965). These systems are very sensitive to salt contamination. Moreover, numerous calibrations must be done due to the drift of the Lyman alpha source;
- Two different kinds of infrared analyzers relying on the passage of air through a tube or in situ measurements (Leuning and Judd 1996), namely:
  - closed-path sensors such as the LI-COR, Inc. Lincoln, Nebraska (LI-COR) 62xx series analyzers, which use the absorption of infrared radiation by water vapor (Hay 1980). Using tube intakes is much less sensitive to optical contamination effects but is rather slow;
  - open path sensors, such as the system described by Auble and Meyers (1992), the OPHIR Corporation, Littleton, Colorado (OPHIR) IR-2000 infrared absorption hygrometer, or the LI-COR's recent LI-7500 gas analyzer. Optical window contamination by salt and particles is a serious drawback.

Moreover, the technique using tunable diode laser (TDL) is promising. The quality of TDL measurements of water vapor at near-infrared wavelengths has recently improved due to the availability of advanced lasers.

Humidity fluctuations can also be deduced from the refractive index measured with a microwave refractometer using a resonant microwave cavity (Gilmer et al. 1965; Ottersten 1969a). Resonant cavity refractometers were developed in the 1960s for studying clear-air turbulence and radio propagation (see, e.g., Coantic and Leducq 1969) and for comparing refractive-index fluctuations with clear-air radar echoes (Ottersten 1969b). The main drawback of the microwave radiometer system was associated with volumic variations of the cavity and, as described by Priestley and Hill (1985), a frequency cut-off located too low in the inertial subrange. Therefore, though the technique was promising for more than 30 yr, it has not been extensively used. In this paper, we analyze how after a few modifications such an instrument can be used to derive the latent heat flux.

First, we briefly describe the background necessary to understand how to obtain humidity and humidity fluxes from the refractive index. In the next section, we give

a technical description of the Centre d'Étude des Environnements Terrestre et Planétaires (CNRS), France (CETP) refractometer and explain how previous technical difficulties have been overcome. We then show how the system has been used in an experiment on an oceanographic ship. Finally, an analysis of data collected during the severe conditions of the Couplage avec l'ATmosphère en Conditions Hivernales (CATCH) experiment in the North Sea (Eymard et al. 1999) and the FETCH (Flux, Etat de la mer et Télédétection en condition de fetCH variable) experiment in the Mediterranean Sea (Hauser et al. 2000) is presented. The method chosen and results are discussed. We conclude with the great potential of this new microwave refractometer for deriving humidity and fluxes.

2. Humidity measurement over the ocean

a. Background on humidity, refractive index, and fluxes

Before investigating more quantitative measurements, it is useful to recall a few basic relations. Vapor pressure e (absolute humidity in hPa) is related to air temperature T (in K), vapor density ρ_v, and gas constant for water vapor R_v by

$$e = \rho_v R_v T. \quad (1)$$

Dry air pressure P_a (in hPa) is related to air temperature T (in K), air density ρ_a, and gas constant for dry air R_a by

$$P_a = \rho_a R_a T. \quad (2)$$

The atmospheric pressure P (in hPa) is given by

$$P = P_a + e. \quad (3)$$

The specific humidity Q is the ratio between the mass of water vapor in an air volume and the total air mass in the same volume:

$$Q = (R_a/R_v)e/[P - (1 - (R_a/R_v))e]$$
$$= 0.622e/(P - 0.378e). \quad (4)$$

The mixing ratio r is the ratio between the mass of water vapor and the dry air mass in the same volume:

$$r = (R_a/R_v)e/(P - e) = 0.622e/(P - e). \quad (5)$$

As $e/P < 0.04$, in the literature, one often finds

$$r \approx Q = 0.622e/P \quad (6)$$

[see, e.g., Stull (1988) for more details about humidity description and units]. Relative humidity RH, often expressed in percentage, is the ratio between air mixing ratio r and air mixing ratio r_w at saturation:

$$\text{RH} = r/r_w = e/e_w, \quad (7)$$

where e_w is the water vapor pressure at saturation.

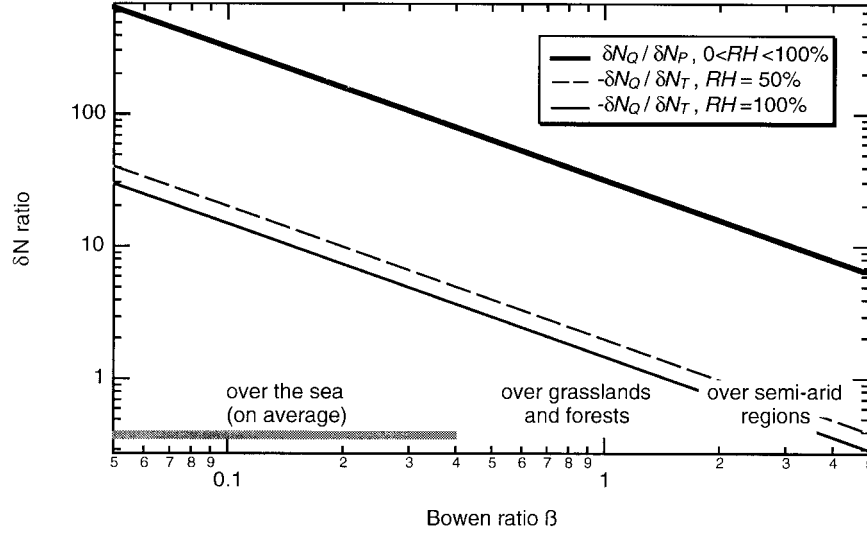The relationship between the refractive coindex N,

FIG. 1. Variation of $\delta N_Q/\delta N_P$ and $\delta N_Q/\delta N_T$ with the Bowen ratio for RH = 50% and 100%.

the refractive index n_r, vapor pressure, atmospheric pressure, and temperature is

$$N = (n_r - 1) \times 10^6 = A(P/T)(1 + Be/T), \qquad (8)$$

where A and B are constant with respect to the wavelength in the radio frequency range. The equation of Smith and Weintraub (1953) has been in standard use for many years:

$$N = 77.6P/T + 3.73 \times 10^5 \, e/T^2. \qquad (9)$$

The overall error in N is less than 0.5 at sea level pressures for very moist air (Thayer 1974). Hence, using the specific humidity given by (4), one gets

$$N = P(77.6/T + 6.0 \times 10^5 \, Q/T^2) \qquad (10)$$

from which, knowing the temperature and the pressure, the specific humidity can be estimated.

b. Relationship between index fluctuation and temperature and humidity fluctuation

Computing the partial derivative relative to pressure, temperature, and humidity,

$$\delta N_p = [(\partial N/\partial P) + (\partial N/\partial Q)(\partial Q/\partial P)]\delta P$$

$$= [77.6/T]\delta P, \qquad (11)$$

$$\delta N_T = (\partial N/\partial T)\delta T$$

$$= P[-77.6/T^2 - 12.0 \times 10^5 \, Q/T^3]\delta T, \quad (12)$$

$$\delta N_Q = (\partial N/\partial Q)\delta Q = P[6.0 \times 10^5/T^2]\delta Q, \qquad (13)$$

and choosing usual ocean surface parameter values such as those found in the Atlantic Ocean ($P = 1013$ hPa, $T = 300$ K, relative humidity RH between 10% and 100%), with a temperature fluctuation $\delta T \approx 1$ K and $\delta P/P \approx 0.1\delta T/T$ so that $\delta P = 34$ Pa [as $\delta P/P$ is considered to be small relative to $\delta T/T$ (Kistler 1959), an upper bound can be used], we derive the following two functions of the Bowen ratio β (Stull 1988, 274–275) related to the humidity by $\delta Q = (Cp/Lv)\delta T/\beta$ (where Cp is the specific heat constant at constant pressure and Lv the latent evaporation heat):

- $\delta N_Q/\delta N_P$ = the ratio between the variation of N due to Q and the variation of N due to P,
- $\delta N_Q/\delta N_T$ = the ratio between the variation of N due to Q and the variation of N due to T.

Figure 1 shows the variation of $\delta N_Q/\delta N_P$ and $\delta N_Q/\delta N_T$ with β. Over the ocean, the actual β range has been evaluated during the FETCH experiment described in section 4a. The representation of $\delta N_Q/\delta N_P$ and $\delta N_Q/\delta N_T$ for 50% and 100% relative humidity shows that the humidity-induced variation is two orders of magnitude larger than that due to pressure and one order of magnitude larger than that due to temperature. This shows the interest of using refractive index fluctuations to derive sea surface humidity fluxes. In the following, capital letters will be used for mean values and lower case letters for fluctuations.

Various methods to obtain evaporation fluxes can be proposed. The classical Eddy Correlation Method (EDM) gives the evaporation flux $\langle wq \rangle$ knowing vertical velocity of air fluctuations w and temperature flux $\langle wt \rangle$ at the same location:

$$\langle wn \rangle = \partial N/\partial Q\langle wq \rangle + \partial N/\partial T\langle wt \rangle, \qquad (14)$$

where $\langle . . . \rangle$ denotes a temporal average. On board a ship, the vertical movement modifies the correlations and cospectra of $\langle wn \rangle$ and $\langle wt \rangle$ within a wide range of timescales and frequencies. The method then requires the knowledge of the ship movement parameters (six degrees of freedom) in order to correct the data for this motion.

A method based on the computation of structure func-

tions has been proposed to derive fluxes by means of a clear-air radar [see, e.g., Gossard (1960) and Rabin and Doviak (1989)]. The idea is to derive surface fluxes from the structure function of index fluctuation C_n^2:

$$C_n^2 = [a^2 C_t^2 + b^2 C_q^2 - 2ab C_{qt}^2], \qquad (15)$$

where C_t^2, C_q^2, and C_{qt}^2 are the structure functions of temperature fluctuations, humidity fluctuations, and temperature and humidity covariance, respectively. This method is particularly attractive if the temperature structure function is directly computed using, for example, acoustic sounders or scintillometers. The inertial-dissipative method, described in section 5 of this paper, is similar; however, it does not use C_{qt}^2, as it is generally not easy to estimate.

3. Technical description of the CETP refractometer

a. Previous designs

The initial design (Crain 1948; Birnbaum 1950) was used to determine the dielectric permittivity of gases. It combines a circular cylindrical "open" cavity operating in the TE_{011} mode near 9.4 GHz with a frequency measurement system. If we fill a cavity, whose refractive index is n_r, with a gas, the resonant frequency will be given by f, which is related to the wavelength λ by

$$\lambda = \mu / n_r f, \qquad (16)$$

where μ is a constant related to the shape of the cavity. If the cavity keeps its shape, λ is constant, and then

$$\Delta f / f = -\Delta n_r / n_r. \qquad (17)$$

The measurement of the refractive index is reduced to a frequency measurement. As N is related to n_r by (8), the integration of (17) gives

$$N = N_0 - (10^6 + N_0)(f - f_0)/f_0 \quad \text{or}$$

$$N = [-(10^6 + N_0)/f_0]f + (10^6 + 2N_0), \qquad (18)$$

where f_0 is related to a given value of N_0. Then, a single calibration point is needed. We have considered this kind of microwave refractometer because of its inherent linearity, even if other types have been developed in the past (Straiton 1964). Another motivation is the reduced effect of moisture and dust particles depositing on the walls, also reported by Straiton (1964).

The frequency measurement system was initially dependent on a sealed reference cavity and a frequency discriminator (Crain 1950) suitable for atmospheric measurements. Later, a voltage-controlled oscillator (VCO) was tuned to a submultiple of the sampling cavity resonance by means of a phase sensitive detector. The VCO frequency (≈ 100 MHz) was then counted (Vetter and Thomson 1971). A major simplification in refractometer design was carried out at Rutherford Appleton Laboratory, Chilton, United Kingdom. (R.A.L.) by eliminating the reference oscillator. A GaAs FET

amplifier was simply connected in series with a sampling cavity (Yilmaz et al. 1983). A microwave frequency counter provided a time resolution of 10 ms.

We have tested this concept and unfortunately found that the system oscillated at a frequency that depended on the phase of the microwave amplifier transfer function. This phase is closely related to the amplifier saturation conditions. Therefore, it was not possible to ensure a low offset relative to zero phase, that is, to safely operate close to resonance.

b. The new design

We have brought together the best of the previous designs.

1) SENSOR UNIT (FIG. 2)

A cavity made with the lowest expansion material was used. This solution has been previously experimented by Corning Glass (Gunderson and Smith 1968). We chose Zerodur-M glass ceramic from Schott Glaswerke (Mainz, Germany) because of its low temperature hysteresis (Haug et al. 1989). The machining and silver plus gold plating was made by Quartex.[1] An already known and proven cavity geometry was used such as the one implemented by the R.A.L. The proportion of end surface area removed is close to 90%, as previously described (Thompson et al. 1959). The circuit comprises a VCO phase-locked on the resonance (Delahaye and Fournet–Fayas 1988).[2] A mechanical design suitable for ground, ship, and airplane operation was employed.

2) CONTROL UNIT

A microwave frequency counter was used, which was able to count a 9.4-GHz signal with a frequency resolution of 100 Hz and a time resolution of 10 ms and included a down converter in order to reduce the final counting range to 0–6 MHz. A high stability crystal oscillator was used to drive a 9.0–9.9-GHz frequency synthesizer with a 1-MHz step size. This synthesizer is useful to adjust the local oscillator frequency of the microwave frequency counter according to the dimensions of different cavity fabrication batches. It is also cheaper to add a synthesizer than to reduce machining tolerances.

In order to study and optimize the residual drift and to make the calibration easier, we have added the following:

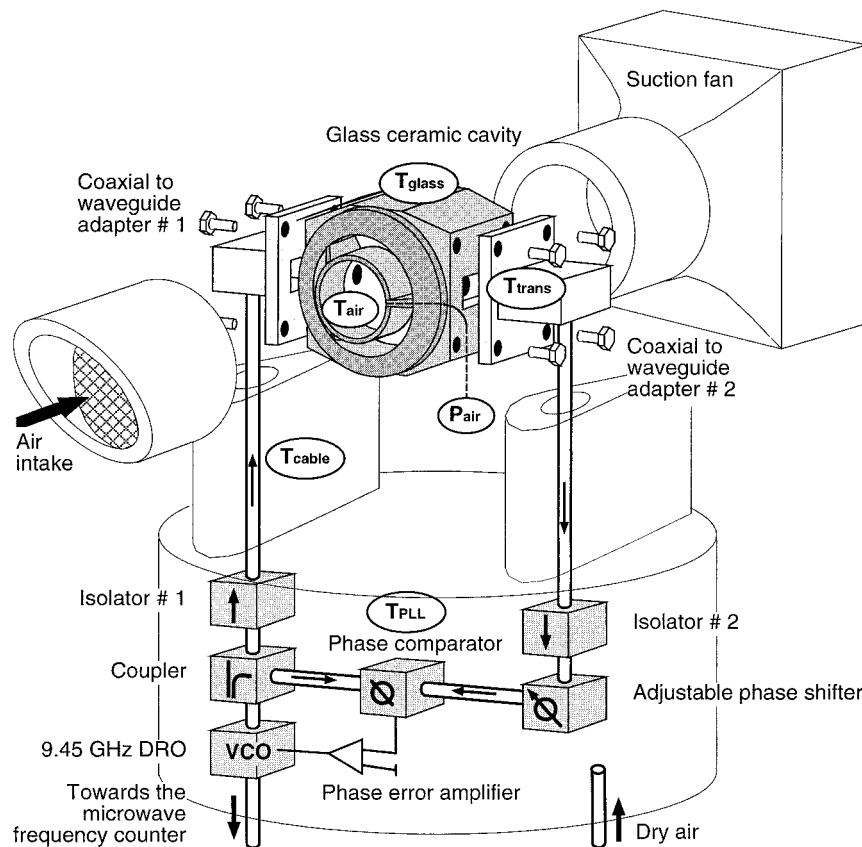• two thermoregulated heating systems around the co-

FIG. 2. The 3D representation of the shipborne refractometer sensor.

axial cables between the cavity and the electronics (T_{cable}) and close to the phase lock circuitry (T_{PLL}),

- an air temperature sensor (T_{air}) made with a 0.25 mm diameter type K thermocouple from Thermocoax (Suresnes, France) and an air pressure sensor (P_{air}) made with a diffused piezoresistive transducer from Endevco (San Juan Capistrano, California),
- an additional temperature sensor made with a 1-mm diameter type K thermocouple successively mounted inside the glass ceramic material (T_{glass}) and on one of the coaxial to waveguide adapters (T_{trans}),
- analog and digital outputs on the control unit.

Because of losses at 9.45 GHz, an external amplifier is used when the length of coaxial cable linking the control unit and the sensor unit exceeds 5 m, allowing a 70-m operating distance.

Two identical models have been built, one for airborne applications and one for shipborne use. The following specific improvements were carried out on the shipborne model:

- In order to avoid condensation around the unventilated parts, dry air can be blown into the electronic box just behind the cavity from a pressure-regulated pump through a drilled SMA test connector.
- The cleanliness of the cavity when the horizontal wind

velocity is too low has lead to the addition of a suction fan in order to suck any particles through quickly. A thin stainless steel mesh attached at the front (Fig. 2) stops the larger ones.

3) DYNAMIC RESPONSE TO THE AIRFLOW ORIENTATION

Using the refractometer for flux measurements on board a ship, the transfer function of the cavity and its angular response were analyzed, since it is not always possible to keep the sensor unit directed upwind. The effect of the presence of the different elements will be discussed below.

The distance response of the instrument was established to be of about $L_r = 1$ m, basedon experimental and theoretical studies (Gilmer et al. 1965), due to the shape and dimension of the system. Thus, the wavelengths smaller than L_r (and therefore frequencies higher than $F_r = U/L_r$, where U is the relative wind speed) are not considered.

The air velocity inside the refractometer is altered by the presence of the protection mesh at the upwind end and by the suction fan at the downwind end. In order to calibrate these effects, laboratory experiments were conducted in a wind tunnel at Institut de Recherche sur
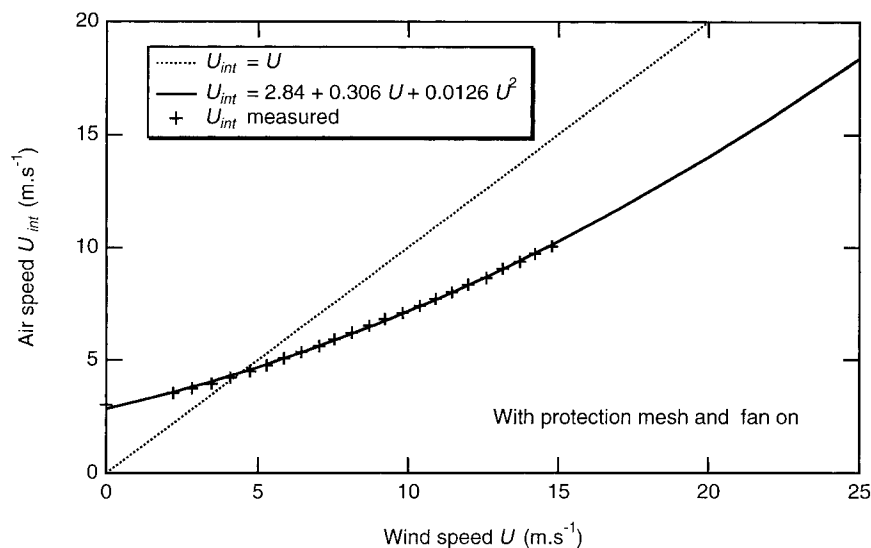
FIG. 3. Variation of the air velocity U_{int} inside the cavity when a wind velocity U is applied (horizontal wind incidence $\alpha = 0$), measured in a wind tunnel at IRPHE.

les Phénomènes Hors Équilibre (CNRS), France (IRPHE). The apparatus was put in the middle of the wind facility, and the air velocity was measured using small hot wire anemometers (DISA 55 M 01: 1 mm $\times$ 3 μm) inside the cavity, U_{int}, and outside the refractometer, U. Wind velocities from 0 to 15 m s^{-1} were applied. Several configurations were tested, with and without the protection mesh and the suction fan. Figure 3 shows the variation of U_{int} with U, with the mesh and the fan installed. At low wind speed ($U < 5$ m s^{-1}), the suction fan induces an increase of the flow, and U_{int} is greater than U. At higher wind speed, the protection grid creates a discharge downstream of the refractometer entrance,

inside the cavity, and the fan is not sufficient enough to evacuate the flow; therefore, U_{int} is lower than U.

The calibration curve $U_{int} = f(U)$ is also shown in Fig. 3. The variable U_{int} depends on the horizontal incidence angle α (the ship is not always pointed into the wind direction, and, for rough sea states, α may vary significantly). In the laboratory wind tunnel, wind measurements were conducted with horizontal incidence angles ranging from 0° to 90°. Figure 4 shows the variation of U_{int} with alpha. There is clearly an effect at high winds and large incidence angle. However, the calibration curve is valid within 10% accuracy for incidence angles lower than 40°. In actual conditions, data with
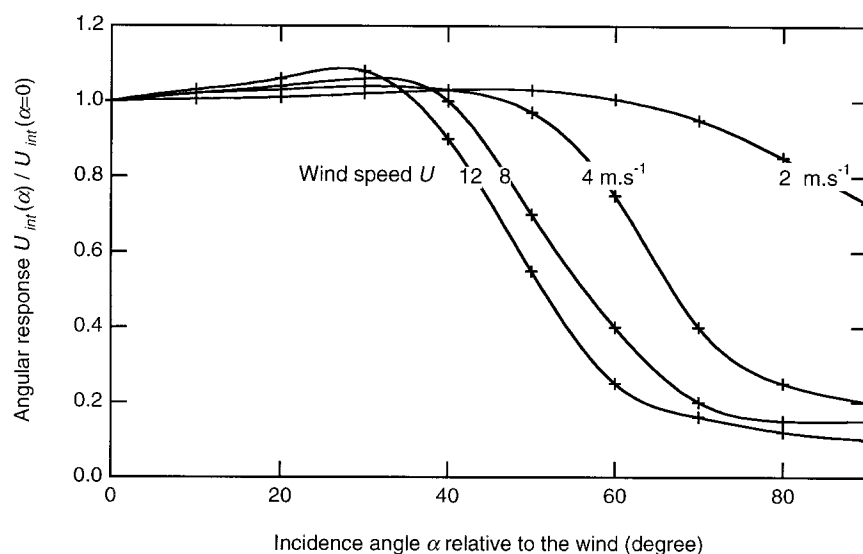

FIG. 4. Variation of air velocity U_{int} inside the cavity with the horizontal wind incidence angle α, measured in a wind tunnel at IRPHE.
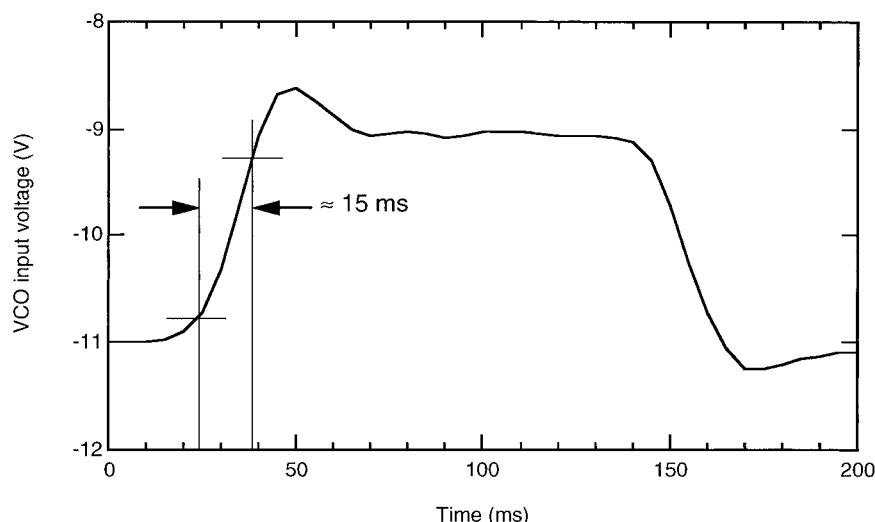
FIG. 5. Variation of the VCO input voltage when a small ball is thrown through the cavity.

alpha greater than a threshold value of 30° were not considered. Although U_{int} is not used in the following computations, it appears that the flow is not disturbed in the angular ranges mentioned above, in spite of the obstacles. Thus, what is measured is indeed N, except for excessive angles. There is no index variation when the fan is turned off.

c. Performance of the new design

1) DYNAMIC PERFORMANCE

Flux measurements mainly require good dynamic performance. If the sample frequency is 50 Hz and the cutoff frequency of the antialiasing filter of the acquisition unit is 25 Hz, the response time of the instrument must be close to 15 ms. In the laboratory, we have adjusted the time constants of the phase locked loop in order to get this value for the rise and fall time, when a small ball is thrown through the cavity (Fig. 5). As the sample volume is not precisely defined on each open side of the cavity, this measurement is not accurate, but it gives an upper limit.

The airborne model flying at 100 m s⁻¹ was used to check the high frequency response by direct comparison with a Lyman-alpha hygrometer (Nacass et al. 1995). On entry into a cloud top, we have observed similar output signals with a delay corresponding to the distance between the locations of both instruments (Fig. 6). The power spectrum from 0.01 to 12.5 Hz is the same for both, and no discrepancy is observed from the $f^{-5/3}$ law during clear air conditions.

2) STATIC PERFORMANCE

The expansion coefficient of the cavity ($\approx 10^{-6}$ K⁻¹) is higher than expected. For applications that need an absolute value of humidity, this aspect is still under development. In the case of flux measurements, it is only required to check the very small influence of drift variations over the power spectrum. In a calibration chamber, we changed the temperature of dry nitrogen around and inside the cavity from 20° to 0°C and measured the difference ΔN between the experimental value of N and the theoretical one. We observed that ΔN varies roughly from 0 to -20 but with a delay of 5 min (Fig. 7). This long delay may be due to the low thermal conductivity of glass ceramics. This means that higher frequency variations of temperature are integrated and thus the drift variations induce negligible errors in the power spectrum over 0.01 Hz.

The dynamic performance corresponds to the slope of the transfer function (18). As N_0 is negligible in comparison with 10^6, this slope is independent of N_0 drifts. The static performance is linked to the term ($10^6 + 2N_0$) and is directly related to the drift of N_0. As this drift has a time constant of several minutes, the refractometer is well suited to applications requiring only variation measurements in a range starting at 0.01 Hz, such as flux determination using the Inertial Dissipative Method (IDM). High frequencies larger than 0.01 Hz are particularly adapted to IDM, since they are much less subject to distortion and ship motion effects than the EDM.

4. Experimental implementation

a. The installation of the refractometer

The shipborne refractometer has been successively installed on two different ships during two international campaigns. The CATCH experiment was part of the Fronts and Atlantic Storm-Track Experiment (FASTEX) program carried out in January and February 1997 in the North Atlantic (Joly et al. 1997; Eymard et al. 1999). The study of energy exchanges between the ocean and
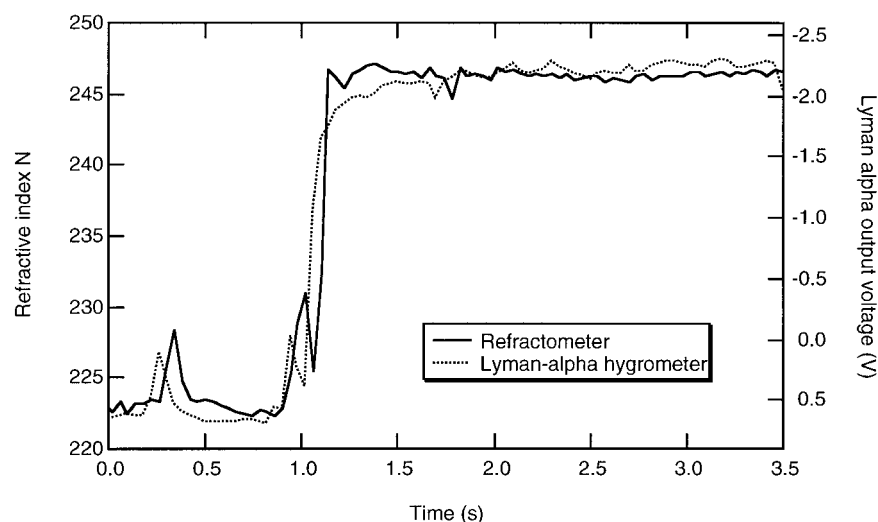
FIG. 6. Comparison between time series measured by a Lyman–alpha hygrometer and the refractometer on entry into a cloud top.

the atmosphere was performed from the R/V *Le Suroit*. The FETCH campaign took place in March and April 1998 in the Mediterranean Sea (Dupuis et al. 1999; Hauser et al. 2000). One of its objectives was the measurement and the parameterization of the turbulent fluxes at the interface between the ocean and the atmosphere. The two CETP refractometers were used, one on the Merlin IV aircraft and the other on the R/V *L'Atalante*.

On a large ship, a good accuracy for atmospheric measurements and especially humidity can be obtained only at the bow at some height above the deck (Blanc 1986; Nacass 1999). Therefore, atmospheric sensors have been mounted on the same 12-m mast on both ships (see Fig. 8 for the implementation on board *L'Atalante*). Three cables link the refractometer sensor and the control unit: a multiplepair cable for the power supply of the sensor and the fan and housekeeping data, a coaxial cable for the 9.4-GHz signal, and an incompressible plastic tube delivering low pressure dry air to the sensor. It would have been preferable to put the control unit close to the sensor, but a waterproof box able to evacuate heat produced by the frequency synthesizer was difficult to design; thus, long cables were used despite the fact that coaxial cable is somewhat expensive.

b. The surrounding instruments

The following atmospheric and radiation sensors were also installed at the top of the mast and at the same level as the Shipborne Refractometer Sensor (SRS):

- a three-axis Ultrasonic Anemometer Sensor (UAS) "research vertical" from Gill Instruments Ltd. The UAS setup in FETCH (Fig. 9) is different from the setup in CATCH. We changed it because of some

perturbation on vertical air velocity due to the support. The acquisition of the analog data outputs of the refractometer is carried out by this unit too;
- two identical ventilated Young radiation shields with temperature and relative humidity sensors HMP 233 from Vaisala;
- two sets of anemometers "wind monitor" from Young for wind speed and horizontal wind direction;
- two digital barometers from Atmospheric Instrumentation Research and from Vaisala;
- a global Solar Irradiance Sensor (SIS) CM3 and a far infrared irradiance sensor CG1 from Kipp and Zonen mounted on a universal joint;
- an optical rain detector ORG 115 from Scientific Technology.

A roll-pitch-heave sensor 335B from TSS (U.K.) Ltd was also mounted at the top of the mast during the FETCH experiment.

The above sensors are complemented for time and positioning with a GPS receiver SV6 from Trimble. Some sensors are located underwater including the following:

- 2 sensors that give the direction and speed relative to the surface in order to calculate the absolute wind parameters: a gyroscope Brown SGB 1000 installed on the gravity center shown in Fig. 7 and an electromagnetic two-axis knotmeter from Alma;
- the sea surface temperature, which is measured at 5 m deep with a platinum hull thermometer fitted inside the sea water aspiration at the stem. The temperature close to the surface is then deduced by means of a model.

The acquisition and recording units are doubled for redundancy. All parameters are continuously recorded, but the data are only valid when the ship is heading upwind. The sampling frequency is 50 Hz for the refractometer
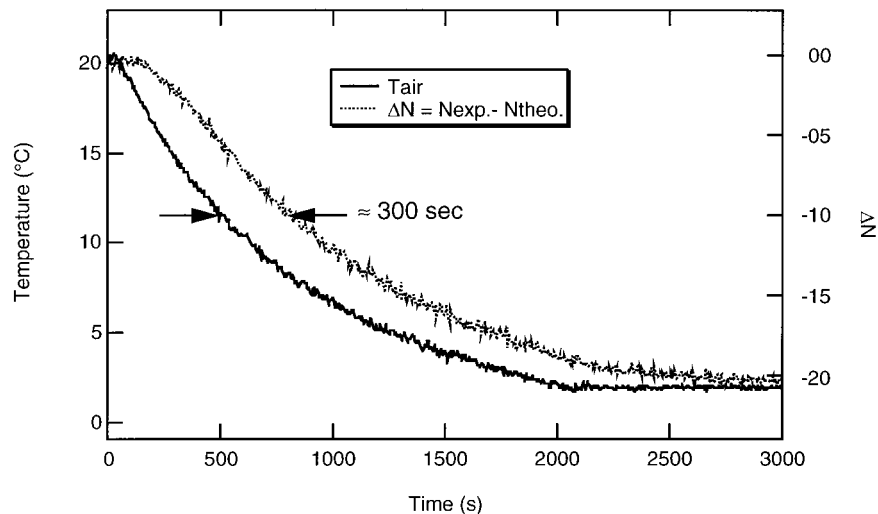
FIG. 7. Comparison of temporal variations of the refractometer error with the temperature during a sudden cooling of the sensor when ventilated with dry nitrogen.

and the sonic anemometer, 1 Hz for GPS, and 0.1 Hz for the others. Because of the availability of analog acquisition inputs on the sonic anemometer, it was simpler for subsequent analysis to use it for recording the refractometer data. This led to the installation of an additional 70-m multiple-pair cable, as can be seen in Fig. 10.

5. Data processing and analysis

a. Flux computation methodology

In this study, the derivation of the turbulent fluxes is based on the IDM, which does not require any motion correction for shipborne measurements. Indeed, dissi-pation rates of the different parameters (here denoted as ε_u, ε_{ts}, and ε_n) are calculated from the high-frequency energy spectra of the signals (u, t_s, and n, respectively, fluctuations of along mean horizontal wind speed U, of sonic temperature T_s, and of air refractive coindex), within the inertial subrange (lower frequencies are disturbed by the ship motion). Application of IDM to standard measurements of wind speed, air temperature, and specific humidity are described in Large and Pond (1981, 1982) for example, while previous developments with a sonic temperature can be found in Larsen et al. (1993) and Dupuis et al. (1997). The method we use with a refractometer can be summarized as follows. First, the dissipation rates are estimated by
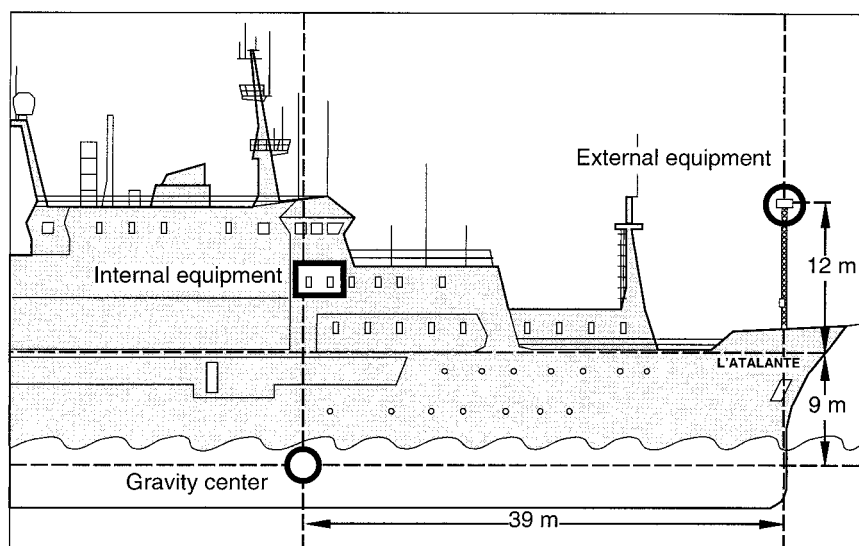

FIG. 8. Sketch of the arrangement of the atmospheric instrumentation during the FETCH experiment.
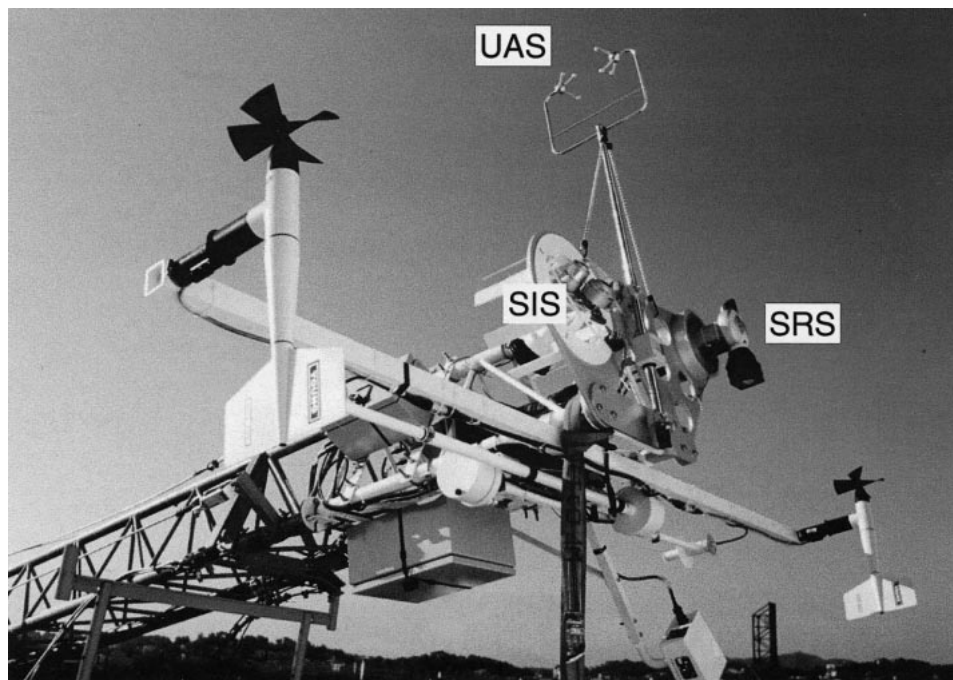
FIG. 9. Atmospheric sensors on top of the 12-m mast during tests before the FETCH experiment: Ultrasonic Anemometer Sensor (UAS), Shipborne Refractometer Sensor (SRS), and Solar Irradiance Sensor (SIS) (photograph by G. Lachaud).
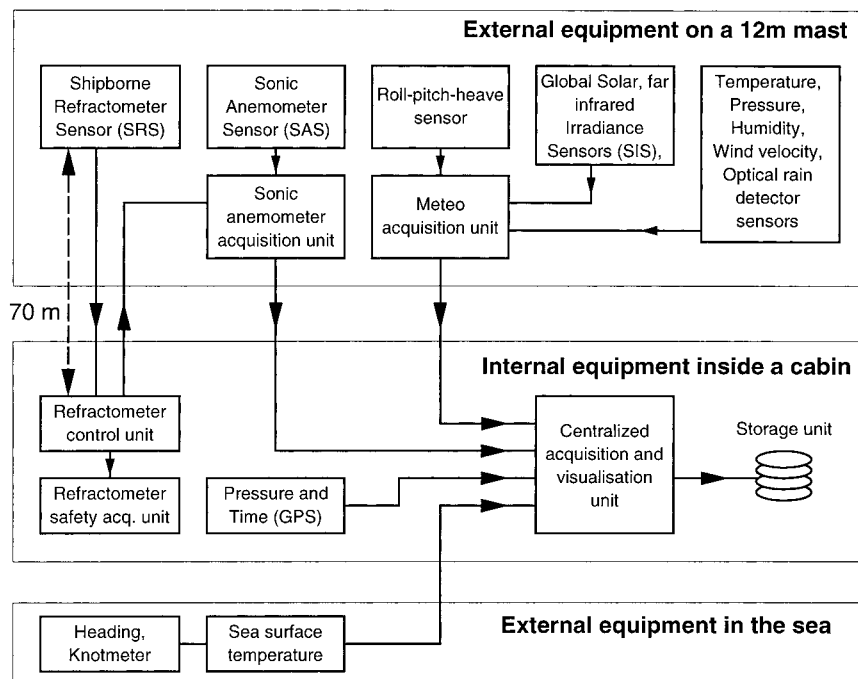

FIG. 10. Block diagram showing the various sensors and acquisition units of the atmospheric instrumentation on the R/V *L'Atalante* during the FETCH experiment.

$$\varepsilon_u = (L_u/\alpha_u)^{3/2}(2\pi/U), \qquad (19)$$

$$\varepsilon_{ts} = (L_{ts}/\alpha_{ts})\varepsilon^{1/3}(2\pi/U)^{2/3}, \qquad (20)$$

$$\varepsilon_n = (L_n/\alpha_n)\varepsilon^{1/3}(2\pi/U)^{2/3}, \qquad (21)$$

where L_u, L_{ts}, and L_n, respectively, are the averages of spectral energy times the 5/3 power of the frequency within an inertial subrange for u, ts, and n. The variable α_i, with $i = u$, ts, and n, is a universal constant. Experimental values of the Kolmogorov constant α_u [Eq. (19)] and of the Obukhov–Corrsin constant α_{ts} [Eq. (20)], are 0.55 and 0.8, respectively. We choose $\alpha_n = 0.8$ as an assumption for a passive scalar. The variable U is the relative wind speed measured by the sonic anemometer.

The spectra have been calculated every half hour, and the inertial subrange is automatically chosen by fitting over several frequency bands. A high-frequency limit of 5 and 25 Hz, respectively, for relative wind speeds of 5 and 25 ms^{-1}, respectively, is associated with the design of the sensor because of the applied response distance of 1 m. Only samples with relative wind direction within $\pm30°$ in the bow are selected (see section 3b). Other applied criteria concern the steadiness of the ship trajectory; the quality of the $-5/3$ slope and the 4/3 ratio of the energy times the 5/3 power of the frequency of v and w, respectively; the horizontal transverse; and vertical transversal velocity fluctuations over u, that is, the assumption of local isotropy (see Dupuis et al. 1997). Figure 11 shows examples of spectra of air refractive index for a wide range of meteorological conditions. This figure emphasizes the very high quality of the high-frequency response of the refractometer. The width of the inertial subrange (zero slope in Fig. 11b) is at least one decade (for wavelengths ranging between 1 and 10 m), which allows one to estimate accurately the dissipation rate of the air refractive index. These dissipation rates are then used to calculate the kinematic fluxes $\langle uw \rangle$, $\langle wt_s \rangle$, and $\langle wn \rangle$ through the budgets of turbulence kinetic energy (TKE) and of variances of both the sonic temperature and the air refractive index. In the budgets, isotropy and stationarity are assumed. Production terms are expressed by the *universal* stratification functions (Φ_m, Φ_{ts}, Φ_n), following the Monin–Obukhov similarity theory:

$$u^* = \{\kappa Z\varepsilon_u/[\Phi_m(Z/L) - Z/L - \Phi_{imb}(Z/L)]\}^{1/3}, \quad (22)$$

$$\langle wt_s \rangle = \text{sign}(\langle wt_s \rangle\text{bulk})[\kappa Zu^*\varepsilon_{ts}/\Phi_{ts}(Z/L)]^{1/2}, \qquad (23)$$

$$\langle wn \rangle = \text{sign}(\langle wn \rangle\text{bulk})[\kappa Zu^*\varepsilon_n/\Phi_n(Z/L)]^{1/2}, \qquad (24)$$

where Z is the height of measurement above the sea surface and $\Phi_{imb}(Z/L)$ is an imbalance function introduced by Yelland and Taylor (1996) and Dupuis et al. (1997) in order to parameterize the vertical transport terms in the TKE budget. The Monin–Obukhov length L can be estimated using a bulk formula

$$L = -T_v u^{*3}/(gk\langle wt_v \rangle), \qquad (25)$$

where $\langle wt_v \rangle$ is the buoyancy flux and t_v is the virtual temperature. The methodology problems related to the IDM method are beyond the scope of this paper. It should, however, be noted that the implementation of the method is still under investigation in order to provide the highest quality of flux estimates. A compromise has to be found between iteration processes ensuring the independence of the flux estimates on initial guesses of L by bulk formulae and a minimization of noise amplification on dissipation rates [see Eymard et al. (1999) for discussion on this point]. Since the signs of $\langle wn \rangle$ and $\langle wq \rangle$ cannot be determined by the IDM, bulk estimates are used instead, following Eqs. (23) and (24). In practice, the probability of obtaining a negative $\langle wn \rangle$ is very small, in contrast to the case of $\langle wt_s \rangle$. The sensible and latent heat fluxes $\langle wt \rangle$ and $\langle wq \rangle$ are then derived:

$$\langle wt_s \rangle = \partial T_s/\partial T\langle wt \rangle + \partial T_s/\partial Q\langle wq \rangle, \qquad (26)$$

where $\partial T_s/\partial T$ and $\partial T_s/\partial Q$ are deduced from $T_s = (1 + 0.518Q)\,T$ and $\langle wn \rangle$ is obtained using Eq. (14). The $\partial N/\partial Q$ and $\partial N/\partial T$ are of the order of 7 and -1.2, respectively. The variability of the ratio and the respective impact of latent and sensible heat flux on the refractive index flux will be discussed in more detail in the following section.

b. First results

Figures 12 and 13 show examples of flux calculations described in the previous section. The spectra are computed over 5-min samples, then averaged over 30-min time periods. The top panels compare latent heat fluxes determined from the IDM (circles) and from a bulk aerodynamic formula, based on Smith et al. (1988) and DeCosmo et al. (1996), as a reference (solid line). If U_{10n} is the neutral wind speed at 10 m height, the neutral drag, evaporation, and heat coefficients C_{dn}, C_{en}, and C_{hn}, respectively, are given by

$$C_{dn} = 0.93 \times 10^{-3} \qquad \text{for } U_{10n} < 5 \text{ m s}^{-1}$$

$$C_{dn} = (0.61 + 0.063U_{10n}) \times 10^{-3} \quad \text{for } U_{10n} > 5 \text{ m s}^{-1}$$

$$C_{en} = C_{hn} = 1.2 \times 10^{-3} \qquad \text{for unstable cases}$$

and

$$C_{hn} = 0.7 \times 10^{-3} \qquad \text{for stable cases.}$$

The bulk fluxes are based upon measurements made with Vaisala HMP 233 temperature and humidity sensors, Young anemometers, and a platinum hull thermometer, which were described in section 4. The two other panels show the meteorological conditions encountered during the two campaigns, CATCH and FETCH, respectively A detailed analysis of flux parameterization would be beyond the scope of this paper, since many other factors, such as flow distortion, can interfere. The reader should refer to other papers dealing
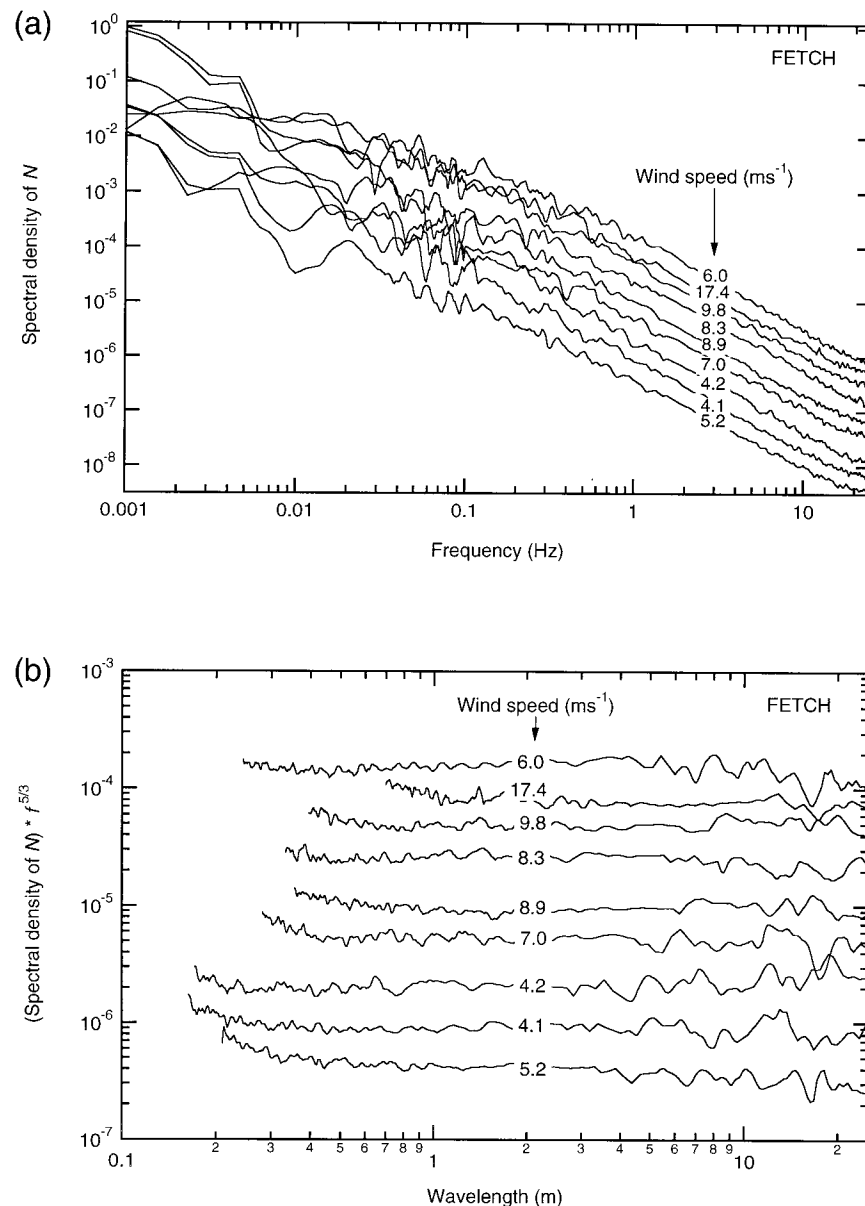
FIG. 11. Example of normalized spectra of air refractive index as a function of (a) frequency or (b) wavelength. The spectra correspond to a large range of wind speed and air temperature minus sea temperature or humidity difference.

with this subject: Eymard et al. (1999) for CATCH and Dupuis et al. (1999) for FETCH. Nevertheless, one can notice that the qualitative agreement between the two estimates of latent heat fluxes is very good. The refractometer thus allowed us to record about 500 samples of latent heat flux for a very wide range of conditions (124 during CATCH and 378 during FETCH). During the CATCH experiment, wind speeds were found to range between 0 and 23 m s^{-1}, and air–sea temperature differences between $+12°$ and $-3°C$ were observed, as displayed in panels 12b and 12c. During the FETCH experiment, wind speeds were found to range between

0 and 18 m s^{-1}, and air–sea temperature differences between $+8°$ and $-7°C$ were observed, as displayed in panels 13b and 13c.

c. Discussion

The refractometer is a very promising sensor for measuring latent heat flux over the ocean because of the very high quality of its high-frequency response, which is important using the IDM and because the sensor has been found to be very reliable and to allow continuous long-term measurements in extreme meteorological
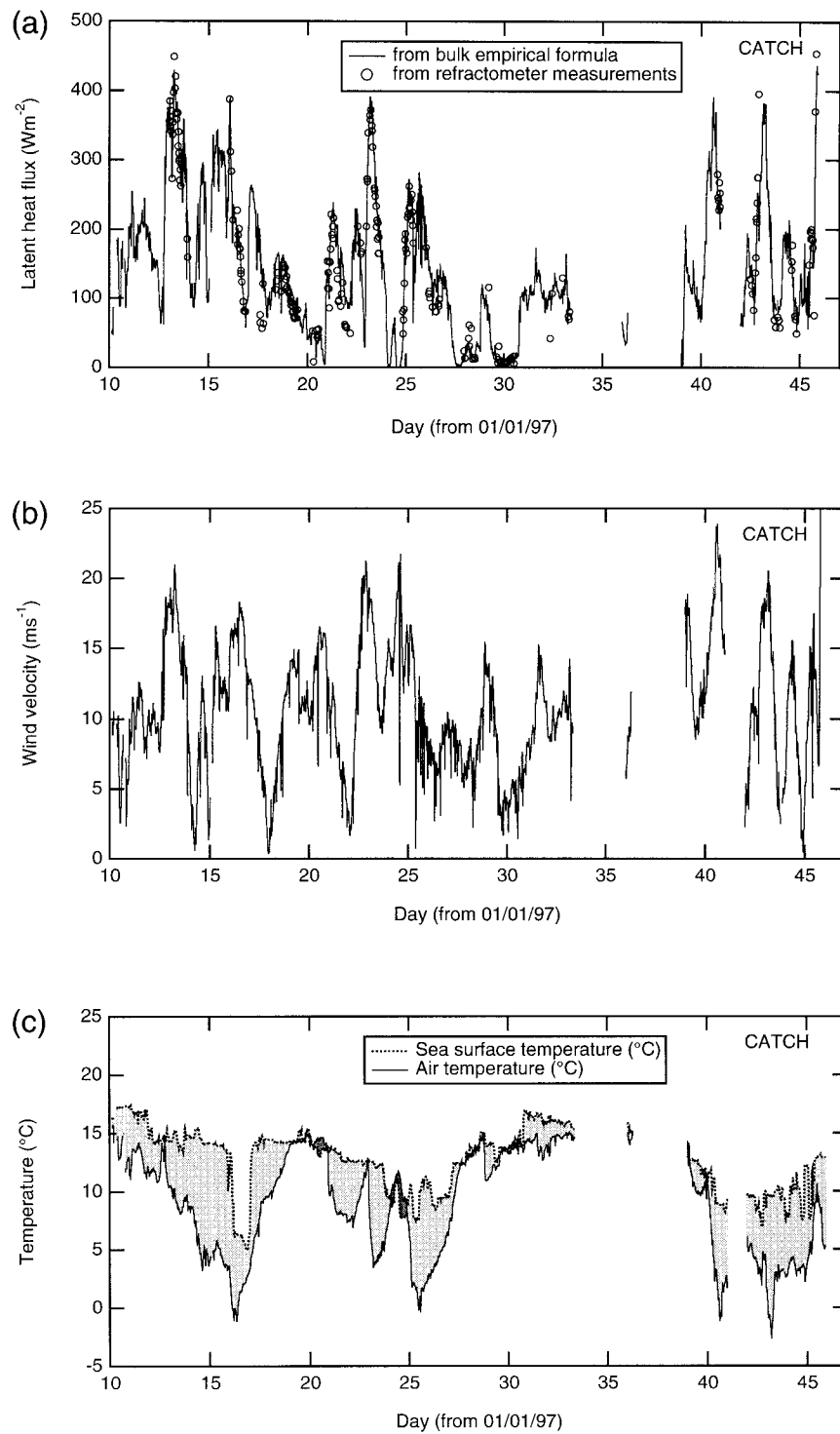
FIG. 12. (a), (b), and (c) Time series of latent heat flux (solid line: bulk empirical formulae; circles: refractometer measurements as described in section 5.1), wind speed, and air plus sea surface temperature, respectively. These data concern the CATCH/FASTEX campaign.
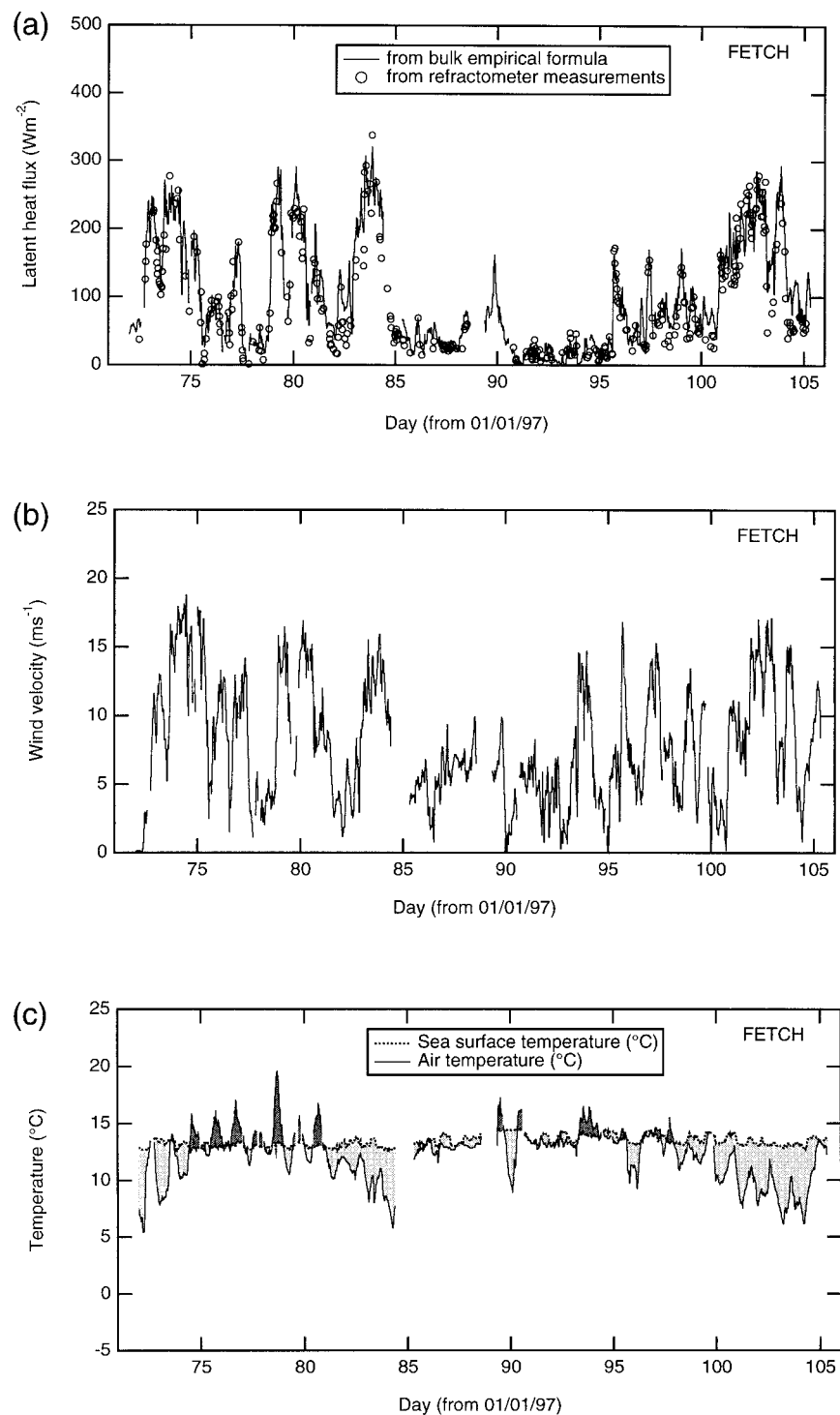
Fig. 13. Same as Fig. 12 but for the FETCH campaign.

conditions such those encountered during the CATCH experiment. The instrument has some limitations however. The most severe limitation of the instrument is related to the perturbation by liquid water inside the cavity in certain meteorological conditions such as driz-

zle, rain, or even air saturated by water vapor. In these cases, the measurements of refractive index are no longer reliable and must be rejected. However, this limitation is common to most fast humidity sensors, and as mentioned in section 2, a system of air suction has been
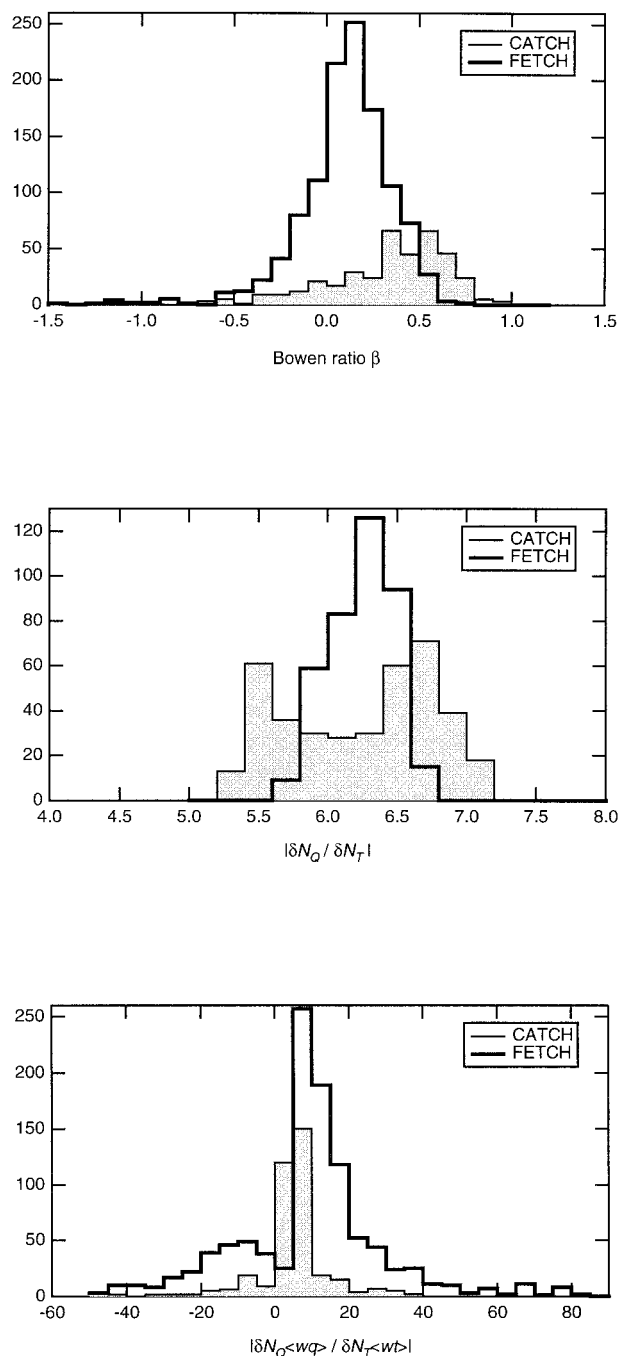
FIG. 14. Histograms of (a) Bowen ratio, (b) $|\delta N_Q/\delta N_T|$, and (c) $|\delta N_Q\langle wq\rangle/\delta N_T\langle wt\rangle|$ for the CATCH and FETCH campaigns.

able number of particles due to ship dynamic effect gives (for a wind speed of 15 m s^{-1} and a friction velocity of 1 m s^{-1}) a warming of 2.5×10^{-8} °C corresponding to a heat flux contribution of 4.1×10^{-4} W m^{-2}, which is negligible. Though the sensor is theoretically not sensitive to such small contamination, some laboratory tests and intercomparison between other flux estimates computed with other instruments should be made to confirm these results.

As the refractometer is not a direct measurement of air humidity, average values of air temperature, humidity, and pressure as well as estimates of sensible heat flux are needed to provide latent heat fluxes [see Eq. (26)]. As shown in Fig. 1, regarding the standard Bowen ratio over the sea (≈ 0.2), the air refractive index flux depends mainly on latent heat fluxes. In almost all cases, bulk estimates of sensible heat flux can be used, but attention should be paid to particular situations with very moist air and/or high air–sea temperature differences. While processing CATCH and FETCH data, we found some samples with high Bowen ratios leading to very comparable contributions of heat and evaporation fluxes in the refractive flux. Figure 14 shows the major differences between these two experiments. Figure 14a shows that the two campaigns are characterized by different Bowen ratio. If a classical value of 0.2 is found to be representative for FETCH, a much higher value of 0.5 is obtained for CATCH. Moreover, although it is of smaller importance, a much higher variability of the ratio of $\delta N_Q/\delta N_T$ is observed during CATCH than during FETCH (panel 14b). Consequently, during FETCH, a very small percentage of samples shows a significant impact of the sensible heat flux in the refractive index flux (less than a few percent of samples have $|\delta N_Q\langle wq\rangle/ \delta N_T\langle wt\rangle|$ less than 5), but this is no longer true for CATCH, where good quality sensible heat fluxes should also be computed for estimating latent heat flux from the air refractive index flux (about 30% of samples have $|\delta N_Q\langle wq\rangle/\delta N_T\langle wt\rangle|$ less than 5) as shown in panel 14c. In these cases, one needs a more accurate estimate of sensible heat flux than using a simple bulk estimate. Unfortunately, as explained in detail in Eymard et al. (1999), during CATCH, the spectra of sonic temperature were found to be of very poor quality and therefore could not used here, contrary to FETCH. Therefore, the latent heat flux estimated during 30% of CATCH period is probably less accurate.

6. Conclusions

We have described a refractometer device, technically improved to analyze refractive index intensity and fluctuations over the sea. This system can be calibrated with a precision of six refractive index units and has been utilized with success to estimate shipborne humidity fluctuations and latent heat flux at sea during the very severe winter conditions of the CATCH 97 experiment in the North Atlantic Sea, with strong wind and sea state

used to allow the refractometer to work very rapidly after the rain or drizzle has stopped. As far as sea spray is concerned, a rough estimate of the number of particles at the level of 17-m height can be estimated (following Makin 1998), and the temperature warming due to particle evaporation and of the consecutive flux perturbation in the cavity can be computed. Using a drastic hypothesis of a multiplicative effect of 100 in the prob-

(particles projection), and during FETCH 98 in the Mediterranean Sea, with strong wind and salt deposition. The refractive index can be considered as a ''passive scalar.'' Its fluctuation density spectrum exhibits a $-5/3$ spectrum range between 0.1 and 10 Hz, providing a very high quality inertial subrange. The refractive index is primarily a function of humidity, less importantly of temperature and pressure. The last term is always negligible. A method is proposed to calculate the latent heat flux based on refractive index flux and an estimate of the sensible heat flux. The latter is generally found to be small enough to justify the use of a bulk parameterization. However, in some meteorological conditions, such as in 30% of CATCH cases, its contribution can be significant. The refractometer does not need calibration for refractive index variations. It is very resistant to salt and other contamination and looks very promising for future routine use to measure humidity fluxes in combination with a sonic anemometer:

The latent heat fluxes derived from CATCH and FETCH by the inertial dissipation method compare well with bulk estimates, and the system has been found to be very robust in high sea states. The good results obtained during these two experiments have allowed the refractometer system to be implemented in subsequent experiments involving French research vessels for obtaining real-time fluxes.

REFERENCES

Auble, D. L., and T. P. Meyers, 1992: An open path, fast response infrared absorption gas analyzer for H_2O and CO_2. *Bound.-Layer Meteor.,* **59,** 243–256.

Birnbaum, G., 1950: A recording microwave refractometer. *Rev. Sci. Instrum.,* **21,** 169–176.

Blanc, T. V., 1986: The effect of inaccuracies in weather-ship data on bulk-derived estimates of flux, stability and sea-surface roughness. *J. Atmos. Oceanic Technol.,* **3,** 12–26.

Coantic, M., and D. Leducq, 1969: Turbulent fluctuations of humidity and their measurement. *Radio Sci.,* **4,** 1169–1174.

——, and C. A. Friehe, 1980: Slow response humidity sensors. *Air-Sea Interaction: Instruments and Methods,* F. Dobson, L. Hasse, and R. Davis, Eds., Plenum Press, 399–411.

Crain, C. M., 1948: The dielectric constant of several gases at a wavelength of 3.2 centimeters. *Phys. Rev.,* **74,** 691–693.

——, 1950: Apparatus for recording fluctuations of the refractive index of the atmosphere at 3.2 centimeters wave-length. *Rev. Sci. Instrum.,* **21,** 456–457.

DeCosmo, J., K. B. Katsaros, S. D. Smith, R. J. Anderson, W. A. Oost, K. Bumke, and H. Chadwick, 1996: Air–sea exchange of sensible heat and water vapor: The HEXOS results. *J. Geophys. Res.,* **101,** 12 001–12 016.

Delahaye, J. Y., and C. Fournet-Fayas, 1988: Appareil de mesure de la fréquence de résonance d'une cavité hyperfréquence. French patent 88-10127, France (Centre National d'Études des Télécommunications, Issy-les-Moulineaux, France).

Dupuis, H., P. K. Taylor, A. Weill, and K. B. Katsaros, 1997: The inertial dissipation method applied to derive momentum fluxes over the ocean during the SOFIA/ASTEX and SEMAPHORE experiments with low to moderate wind speeds. *J. Geophys. Res.,* **102** (C9), 21 115–21 129.

——, C. Guérin, A. Weill, and D. Hauser, 1999: Heat flux estimates by the inertial dissipation method during the FETCH experiment. *The Wind Driven Air-Sea Interface: Electromagnetic and Acoustic Sensing, Wave Dynamics and Turbulent Fluxes,* M. L. Banner, Ed., 297–304.

Eymard, L., and Coauthors, 1999: Surface fluxes in the North Atlantic current during CATCH/FASTEX. *Quart. J. Roy. Meteor. Soc.,* **125,** 3563–3599.

Gilmer, R. O., R. E. McGavin, and B. R. Bean, 1965: Response of NBS microwave refractometer cavities to atmospheric variations. *Radio Sci.,* **69D,** 1213–1217.

Gossard, E. E., 1960: Power spectra of temperature, humidity and refractive index from aircraft and tethered balloon measurement. *IEEE Trans. Antennas Propag.,* **3,** 186–201.

Gunderson, L. C., and D. M. Smith, 1968: A highly temperature-stable microwave resonator. *Appl. Opt.,* **7,** 805–812.

Haug, R., A. Klaas, W. Pannhorst, and E. Rodek, 1989: Length variation in Zerodur M in the temperature range from $-60°C$ to $+100°C$. *Appl. Opt.,* **28,** 4052–4054.

Hauser, D., H. Dupuis, X. Durrieu de Madron, C. Estournel, C. Flamand, J. Pelon, P. Queffelou, and J. M. Lefèvre, 2000: La Campagne FETCH; étude des échanges océan/atmosphère dans le Golfe du Lion. *La Météor.,* **8,** 14–31.

Hay, D. R., 1980: Fast-response humidity sensors. *Air-Sea Interaction: Instruments and Methods,* F. Dobson, L. Hasse, and R. Davis, Eds., Plenum Press, 413–432.

Joly, A., and Coauthors, 1997: The Fronts and Atlantic Storm-Track Experiment (FASTEX): Scientific objectives and experimental design. *Bull. Amer. Meteor. Soc.,* **78,** 1917–1940.

Kistler, A. L., 1959: Fluctuation measurements in a supersonic turbulent boundary layer. *Phys. Fluids,* **2,** 290–296.

Large, W. G., and S. Pond, 1981: Open ocean momentum flux measurements in moderate to strong winds. *J. Phys. Oceanogr.,* **11,** 324–336.

——, and ——, 1982: Sensible and latent heat flux measurement over the ocean. *J. Phys. Oceanogr.,* **12,** 464–482.

Larsen, S. E., J. B. Edson, C. W. Fairall, and P. G. Mestayer, 1993: Measurement of temperature spectra by a sonic anemometer. *J. Atmos. Oceanic Technol.,* **10,** 345–354.

Leuning, R., and M. J. Judd, 1996: The relative merits of open- and closed-path analysers for measurement of eddy fluxes. *Global Change Biol.,* **2,** 241–253.

Makin, V. K., 1998: Air-sea exchange of heat in the presence of wind waves and spray. *J. Geophys. Res.,* **103** (C1), 1137–1152.

McKay, D. J., 1978: A sad look at commercial humidity sensors for meteorological applications. Preprints, *Fourth Symp. on Meteorological Observations and Instrumentation,* Denver, CO, Amer. Meteor. Soc., 7–14.

Nacass, P., 1999: Utilisation de la modélisation des écoulements aérodynamiques pour la mesure atmosphérique à bord du navire océanographique *L'Atalante.* Tech. Rep. Météo-France/CNRM/CAM 22, 132 pp. [Available from Centre d'Aviation Météorologique, Brétigny, France.]

——, C. Abonnel, H. Bellec, M. Morera, and J. Y. Delahaye, 1995: Comparative measurements of in-flight humidity sensors on the Meteo-France Merlin-IV. Preprints, *Ninth Symp. on Meteorological Observations and Instrumentation,* Charlotte, NC, Amer. Meteor. Soc., 430–433.

Ottersten, H., 1969a: Atmospheric structure and radar backscattering in clear air. *Radio Sci.,* **4,** 1179–1193.

——, 1969b: Radar backscattering for the turbulent clear atmosphere. *Radio Sci.,* **4,** 1251–1255.

Priestley, J. T., and R. J. Hill, 1985: Measuring high-frequency hu-

midity, temperature and radio refractive index in the surface layer. *J. Atmos. Oceanic Technol.,* **2,** 233–251.

Rabin, R. M., and R. J. Doviak, 1989: Meteorological and astronomical influences on radar reflectivity in the convective boundary layer. *J. Appl. Meteor.,* **28,** 1226–1235.

Smith, D. S., and Coauthors, 1988: Sea surface wind stress and drag coefficients: The HEXOS results. *Bound.-Layer Meteor.,* **60,** 109–142.

Smith, E. K., and S. Weintraub, 1953: The constants in the equation for atmospheric refractive index at radio frequencies. *Proc. IRE,* **41,** 1035–1037.

Straiton, A. W., 1964: Measurement of the radio refractive index of the atmosphere. *Advances in Radio Research,* J. A. Saxton, Ed., Academic Press, 2–52.

Stull, R. B., 1988: *An Introduction to Boundary Layer Meteorology.* Kluwer Academic Publishers, 666 pp.

Thayer, G. D., 1974: An improved equation for the radio refractive index of air. *Radio Sci.,* **9,** 803–807.

Thompson, M. C., Jr., F. E. Freethey, and D. M. Waters, 1959: End plate modification of X-Band TE011 cavity resonators. *IRE Trans. Microwave Theory Tech.,* **7,** 388–389.

Tillman, J. E., 1965: Water vapor density measurements utilizing the absorption of vacuum ultraviolet and infrared radiation. *Humidity and Moisture,* A. Wexler, Ed., Vol. 1, Reinhold, 428–443.

Vetter, M. J., and M. C. Thompson Jr., 1971: Direct-reading microwave refractometer with quartz-crystal reference. *IEEE Trans. Instrum. Meas.,* **20,** 58.

Yelland, M. J., and P. K. Taylor, 1996: Wind stress measurements from the open ocean. *J. Phys. Oceanogr.,* **26,** 541–558.

Yilmaz, U. M., G. R. Kennedy, and M. P. M. Hall, 1983: A GaAs FET microwave refractometer for tropospheric studies. *Proc. AGARD Conf.,* CP-346, Norway, 9.1–9.5.